STAR Note 171
STAR SILICON DRIFT DETECTORS
Detector Tests

J.R. Hall, A. French,
R. Bellwied, C. Pruneau, V.L. Rykov, and W.K. Wilson
Department of Physics and Astronomy
Wayne State University
Detroit MI 48201

May 6, 1994

Abstract

The purpose of this note is to report on the present status and give an overview of the Silicon Drift Detector (SDD) testing for STAR. Measurements of drift time, signal amplitude, and signal width as functions of drift distance are presented and discussed. Measurements of detector precision in both the drift and anode directions are shown along with the effects of temperature changes. Differential nonlinearities in the drift time are also shown.

The prototype SDDs for STAR were designed by Pavel Rehak [1] and produced by members of the instrumentation group (Hobie Kraner et al.) at Brookhaven National Laboratory. After basic electrical tests at BNL some of these detectors were sent to the then three STAR member SDD labs (Ohio State University, LBL, and Wayne State University) for more extensive evaluation.

We report here on the results of tests of the second production run of STAR SDD prototypes (STAR1 SDDs). These detectors are 4cm $\times$ 4cm linear silicon drift detectors with an anode pitch of 250μm and a cathode pitch of 120μm. The silicon for these detectors was selected for its donor concentration. Of the six devices started in the production, one was broken during processing and five were completed and sent for testing. With exceptions (discussed below) these devices have exhibited excellent large scale drift characteristics and three of them are to be used in a beam test later this year. However, the main focus of this report is on the deviation of these very complicated detectors from the ideal. Some of the tests reported below examine the response of these detectors on a small scale. We wish to reemphasize that to date the results of our tests have been very encouraging and that these detectors appear to be quite practical for our purposes. The results presented below should be used to guide the production of future generations of detectors.

SDD labs

Figure 1 shows a representation of the WSU detector test station. At present, the WSU lab is built around a Tektronix TDS 540 1GS/s digital oscilloscope that is used as a fast waveform digitizer to sample the the SDD's output signals, an EG&G diode laser of wavelength 921nm used to simulate a charged particle hitting the detector, and a stepping motor controlled X-Y table capable of sub-micron step sizes which is used to position our detector under the laser. Also a Keithley 617 programmable electrometer is used for accurate voltage and current measurements and which when connected to a thermistor is used to continuously monitor the detector temperature during data runs. All four of these devices are connected to a PC for readout and control. This allows us to make prolonged programmed data runs over the detector's surface.

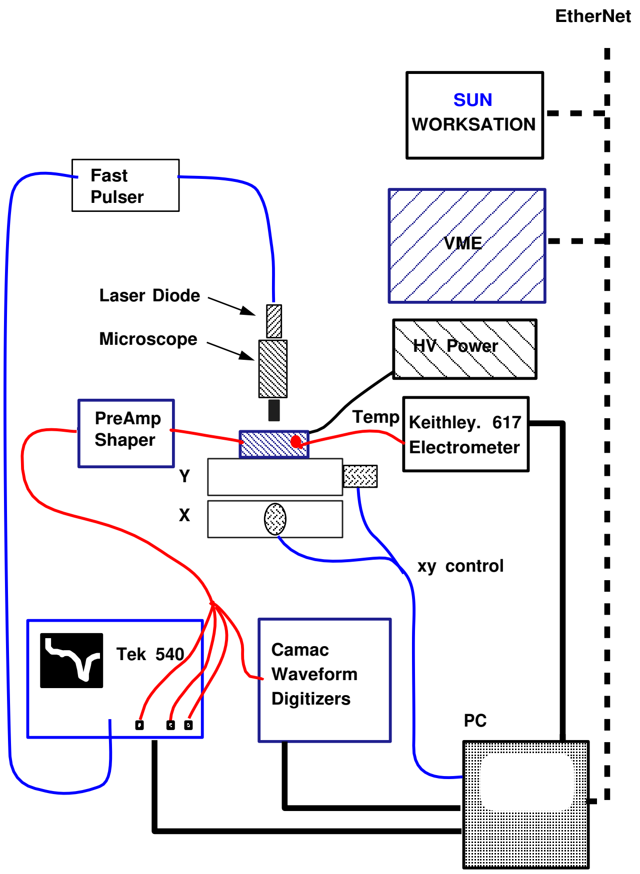

Figure 1: Schematic layout of the Silicon Drift Detector Testing Station.

All of the STAR SDD labs are similar in form but there are differences in components. The labs at LBL and Ohio State use lasers which emit at a wavelength of 1060nm; just where the silicon starts to become transparent. The light from these lasers penetrates the silicon and leaves a 'line' of ionization through the detector, while the lasers used at WSU and BNL emit light which is absorbed just below the surface. However, the BNL and WSU lasers are capable of high pulse rates allowing faster data acquisition. Much of the LBL data was taken using a switched capacitor array (SCA) which has a lower sampling rate. In the discussions below these differences will be mentioned only where they are significant to the data.

At WSU the laser diode is focused onto the SDD through the objective of a microscope. The focused spot size is about 25 ± 5 microns long by 15 ± 5 microns wide and has a time duration of $\approx 8 \pm 1$ns. This laser has a high repetition rate and excellent long term amplitude stability. However, because of its wavelength, the light from the laser is absorbed near the surface of the SDD; in contrast a charged particle creates ionization all along its path through the detector.

Bias and Drift

When the detectors are biased using only their own implanted resistor chains, the resulting potential is not linear along the detector as desired but rather has a quadratic dependence on position as is shown in fig. 2A. Such a dependence would result if at each equipotential strip a fixed amount of current were leaking from the resistor chain to a separate return path (surface currents ?).

$$I(l) = I_0 + l \times i$$

then

$$\mathcal{E}(l) = \Sigma_{n=0}^{l} R_n I(n) = R \Sigma_{n=0}^{l} (I_0 + ni) = R(l I_0 + \frac{l(l+1)}{2})$$

$$\mathcal{E}(l) = V_0 l + \Delta \mathcal{E} l^2$$

where $\mathcal{E}(l)$ the bias potential as a function of strip number, l is the strip number, $R_n = R$ is the value of the implanted resistors, I_0 is the resistor current left at the anode end of the detector, and i is the amount of current that is lost to 'surface currents' at each strip. This leakage may ultimately limit the resistance of the detector's own internal resistance chain. High resistance reduces the heat that must be removed from the detector but the smaller current flowing in the resistor chain would more easily affected by leakage currents. Even with an external resistor chain the regions between contact with the external chain would be susceptible to local sagging if the resistance of the internal chain were too high.

A measured drift time versus drift distance with such biasing is shown in figure 2B.

When the detector is biased in this manner, the measured relationship between drift time and distance is logarithmic as one would predict;

$$v_d(x) = \mu E(x) = \mu \frac{d\mathcal{E}(x)}{dx} = \mu(E_0 + 2l\Delta E)$$

but

$$t_d(x) = \int_0^x v_d(x')^{-1} dx' = \int_0^x \mu^{-1} (E_0 + 2l\Delta E)^{-1} dx'$$

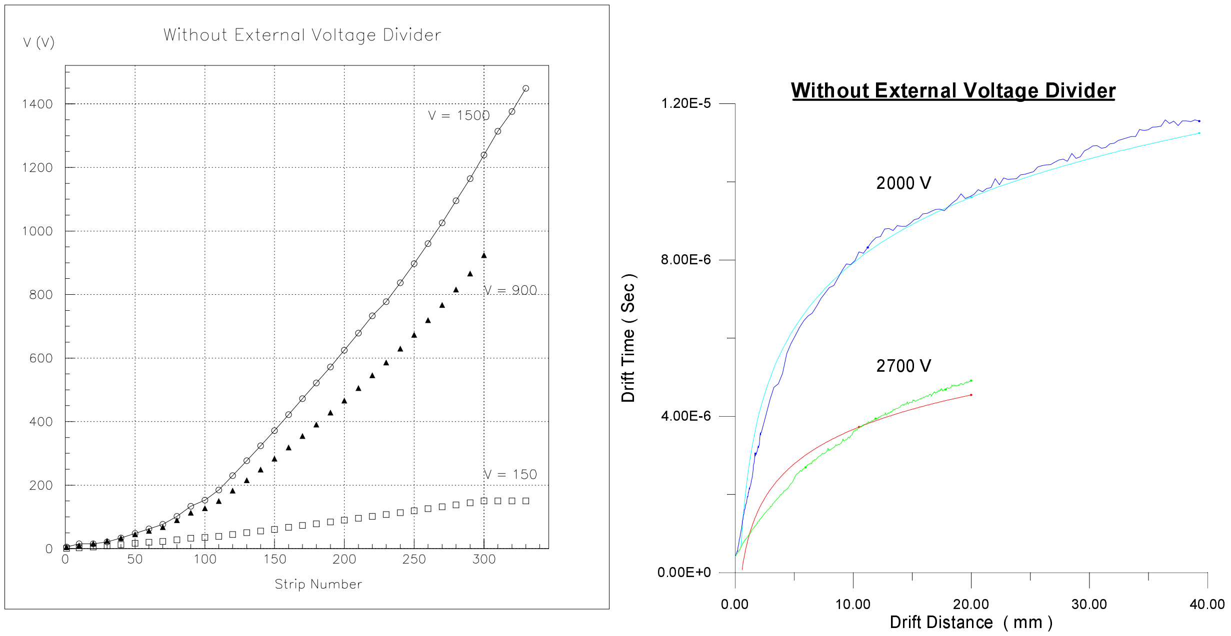

Figure 2: A: Nonlinear bias of detector #395 using only internal resistor chain. B: Drift time versus drift distance for detector #395 biased with internal resistor chain. The dotted curves are logarithmic fits to the data.

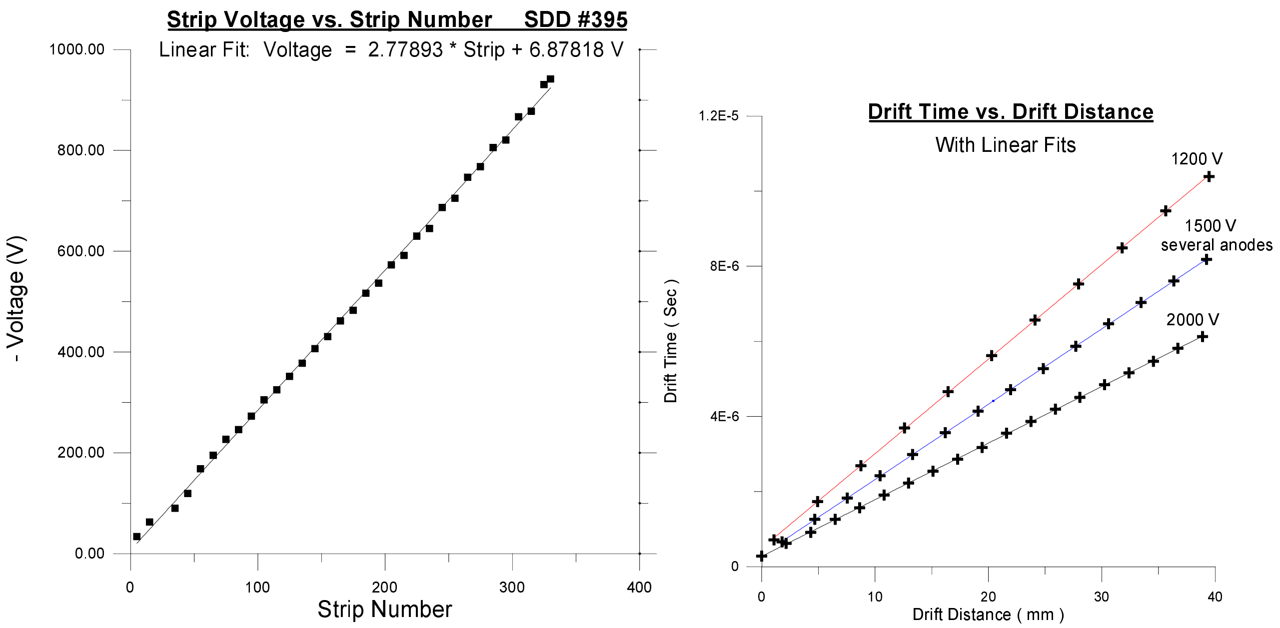

Figure 3: A: Linear bias of detector #395 using external resistor chain. B: Drift time versus drift distance for detector #395 biased with external resistor chain.

$$t_d(x) \propto \ln\left(\frac{E_0 + 2l\Delta E}{E_0}\right) \propto \ln(A + Bl)$$

where x is distance along the drift direction ($x = l \times$ strip spacing), l is the strip number, $v_d(x)$ is the drift velocity as a function of distance, $t_d(x)$ is the time to drift a distance x, μ is the silicon mobility, and $\mathcal{E}(x)$ is the bias voltage (see above) as a function of x. The dotted curves in figure 2B are a logarithmic fit to the data.

A linear relationship between drift voltage along the detector and distance is achieved when using an external voltage divider chain to support the detector's own internal chain as is shown in fig. 3A. The resulting drift for several voltages is shown in fig. 3B. On this scale these data show a linear relationship between drift time and drift distance which is what we would require for a workable detector. The drift velocity also scales with the applied bias. In contrast an example of a detector that did not drift well (detector #405) is shown in figure 4. A 'jump' occurs in the drift time versus distance curve at approximately six millimeters drift distance. We will return to this detector later.

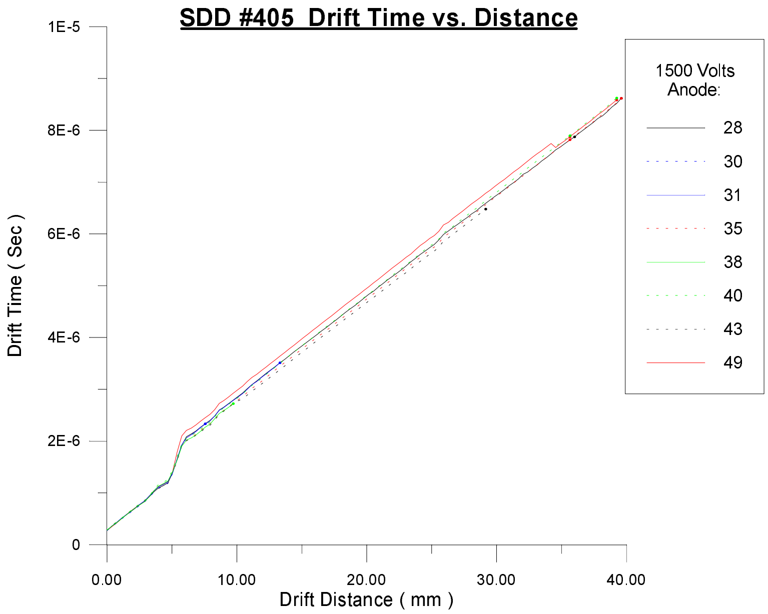

Figure 4: A large nonlinearity is seen in the drift times versus distance curve for detector #405 at approximately six millimeters drift distance.

Drift cloud and Analog Signal

An example of the SDD's analog signal is shown in figure 5. Here we see the signal on three adjacent anodes after a drift of 30mm with 2000V bias applied to the detector (note that the vertical scale is not the same for each channel). The drift velocity in this

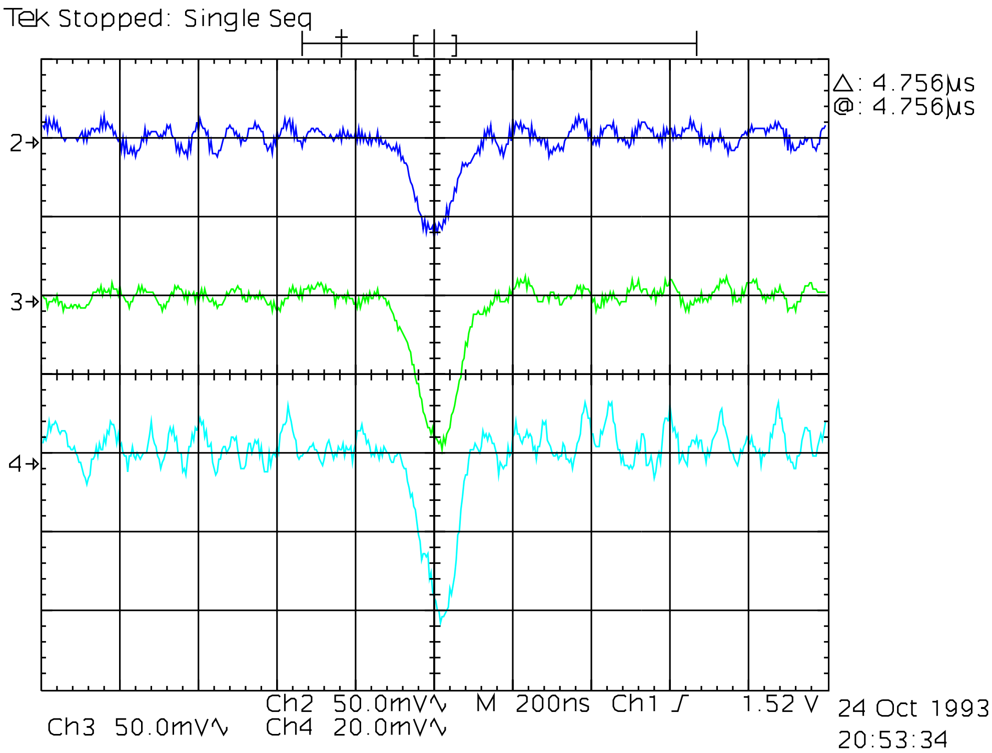

Figure 5: Analog pulses after a drift of 30mm as seen on the digital oscilloscope.

case is about $5\mu m/ns$ placing the start time off of scale to the left. These signals are from a single laser pulse (not averaged signals) and the background noise seen is typical for our system. The noise is measured to be about 5mV rms. The signal from the laser was centered with respect to the central anode and creates an electron cloud roughly equivalent in charge to that from a minimum ionizing charged particle.

The signals were fit to a Gaussian and the centroids (drift time), amplitudes, and sigma (widths) determined from the fit were recorded. Alternatively for some measurements data from several laser pulses were averaged in the digital scope and then fit to a Gaussian. Averaging reduces the effects of noise.

The drifting distribution of electrons is expected to be described by the two dimensional Gaussian;

$$Q_n(y,x,t) = \frac{Q_0 e^{-t/\tau}}{2\pi\sigma_x\sigma_y} e^{-(x-(x_0-v_d t))^2/2\sigma_x^2} e^{-(y-y_0)^2/2\sigma_y^2} .$$

The electron cloud is drifting toward the anodes with a velocity v_d which is determined by the properties of the silicon and the bias voltage. The arrival of charge at a given anode should be described by the following formula;

$$\frac{dQ_n(y,t)}{dt} = \frac{Q_0 e^{-t/\tau}}{2\pi\sigma_x\sigma_y} e^{-(t-t_0)^2/2\sigma_t^2} v_d \int_{-\Delta/2}^{+\Delta/2} e^{-(y-y_0)^2/2\sigma_y^2}\, dy \; .$$

Where $v_d t_0 = x_0$, y_0 is the lateral displacement of the center of the charge cloud from the center of the anode in question, and Δ is the anode spacing (250μm). We have allowed for different widths of the electron cloud in the x (drift) and y (anode) directions ($\sigma_t = \sigma_x / v_d$) and included the possibility of charge recombination ($e^{-t/\tau}$).

The widths in the above equations are time dependent;

$$\sigma_i^2 = \mathcal{F}(\sigma_0^2, 2D_i t, C_i(t, Q_0, \sigma_i(0)) \; .$$

They have a diffusion component (D), a Coulomb component (C) which itself depends on the initial charge distribution Q_0, and a time zero component (σ_0). The Coulomb component is expected to dominate when the charge density is high and be superseded by the diffusion component as the cloud expands. The time zero component should reflect the initial size of the electron cloud and in the time direction the response time of the electronics. As the Coulomb component is not a simple function of time nor distance, it is often incorporated as a part of σ_0 for sufficiently large drift times;

$$\sigma_i^2 = \sigma_0^2 + 2D_i t \; .$$

For the fits described above, we use the reduced equation;

$$\frac{dQ_n(y,t)}{dt} = A_n e^{-(t-t_0)^2/2\sigma_{t_0}^2} \; ,$$

The derived integrated signal strength ($A_n \times \sigma$ is proportional to the total charge in an anode), amplitude (A_n), and sigma (σ_t) are shown in figures 6, 8, and 9 as a function of drift distance for several bias voltages.

The responses shown are well behaved and evidence the diffusion of the charge cloud as it drifts toward the anode. The measured sigma at zero drift distance is consistent with the shaping time of the electronics ($\approx 35ns$ for preamp and shaper). The centroid (drift time) measurements are very robust with those of amplitude and sigma being increasingly less so as witnessed by the scatter shown in figures 8–9. Amplitude measurements are subject to surface effects (dust, reflectivity, trapped charge, etc.). The $A \times \sigma$ figure (fig. 6) shows the increased sharing of the charge with longer drift distance. Because we sum only over three anodes in this figure (top curve) we do not collect all of the charge cloud and the sum diminishes slowly. However, preliminary data from LBL summing over many anodes (fig. 7) would indicate very little if any loss of charge with drift. This result would indicate that we can ignore charge recombination effects.

Measurements are shown in figures 4, 6, 10, and 11 for detector #405. The signal amplitude for this detector (fig. 10) drops sharply at the same point where its time vs. distance curve (fig. 4) shows a jump. The drop in amplitude is so abrupt and severe as

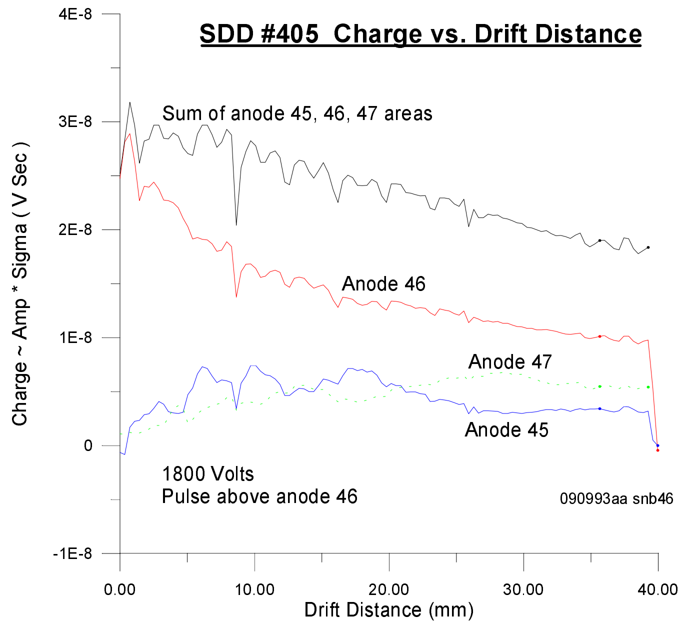

Figure 6: Total charge ($A \times \sigma$) from the centered anode and those on either side as a function of drift distance. The top curve is the sum of the three anodes.

to make the detector nearly useless. However; at that same point the width of the signal (fig. 11) is seen to increase and in such a manner that $A \times \sigma$ (fig. 6) is nearly undisturbed; the total charge in the cloud is conserved.

A clue to what is happening is shown in figure 12. Here we show the current that the external resistor chain is supplying to the detector as a function of distance (strip number). At the point where the amplitude and sigma jumps occur, a large amount of current is being supplied to the detector to maintain voltage. It would appear that an electrical short on the detector has occurred leading to a constant instead of linear drift voltage over a portion of the detector. Because of limiting resistors between the external voltage chain and the detector, the external circuit can not compensate for this 'short'. This low volt gradient region causes the induced drift speed of the electron cloud to drop to a very low value in that region; causing the electrons to pile-up on themselves, sharply increasing the local charge density, and greatly enhancing the component of diffusion caused by Coulomb repulsion. An inspection of this detector under a microscope could find no visible defects.

Precision and Widths

A measurement of detector precision in the drift direction was made by taking a series of single-shot (one laser pulse) measurements of the drift time while at a fixed position (30mm from the anode) and observing the scatter in the results. During these measurements the temperature at the detector was monitored with a thermistor. Some

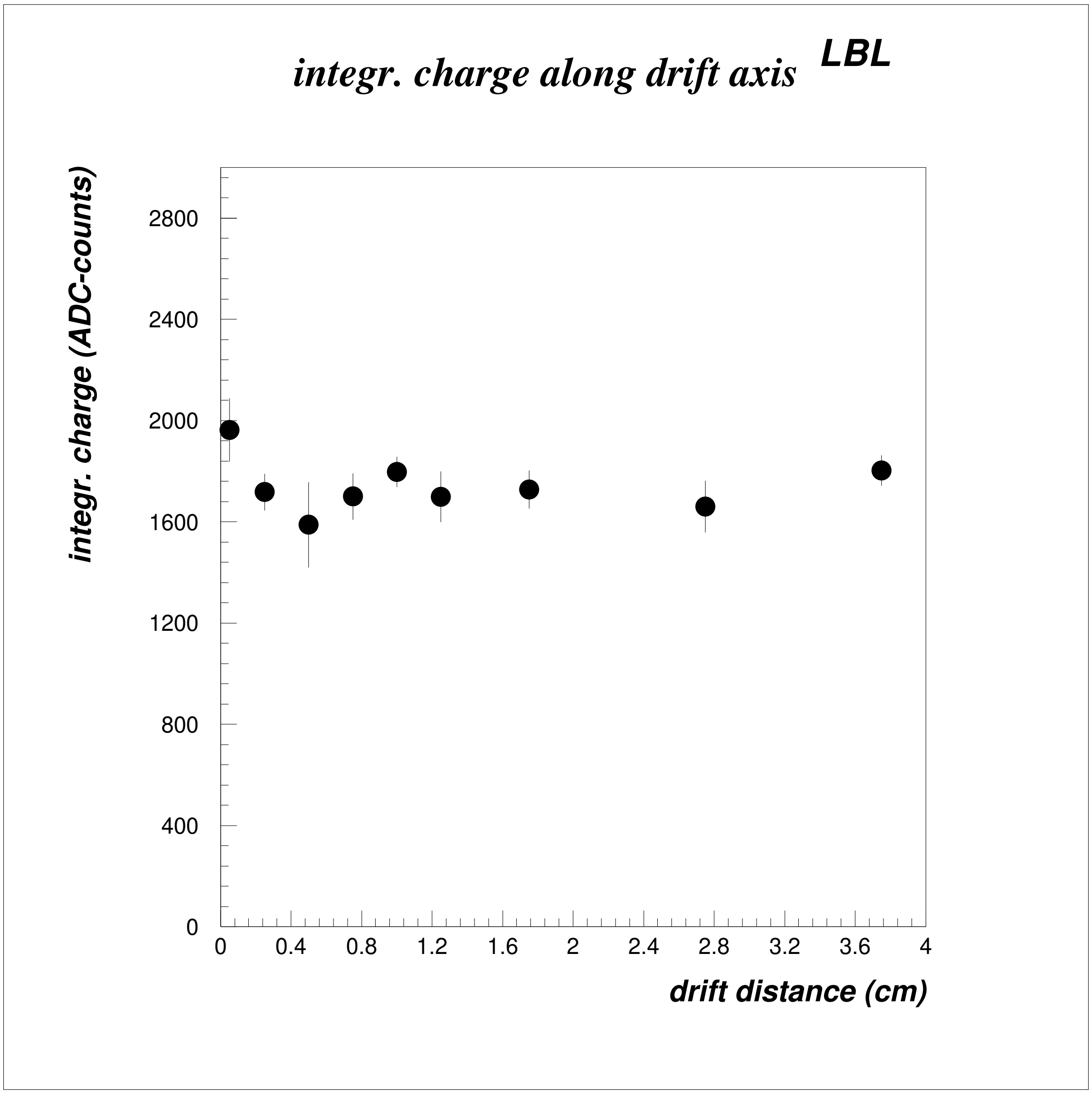

Figure 7: LBL data showing total charge ($A \times \sigma$) from the sum of several anodes as a function of drift distance. This data indicates very little loss of charge with distance. This figure supplies by LBL.

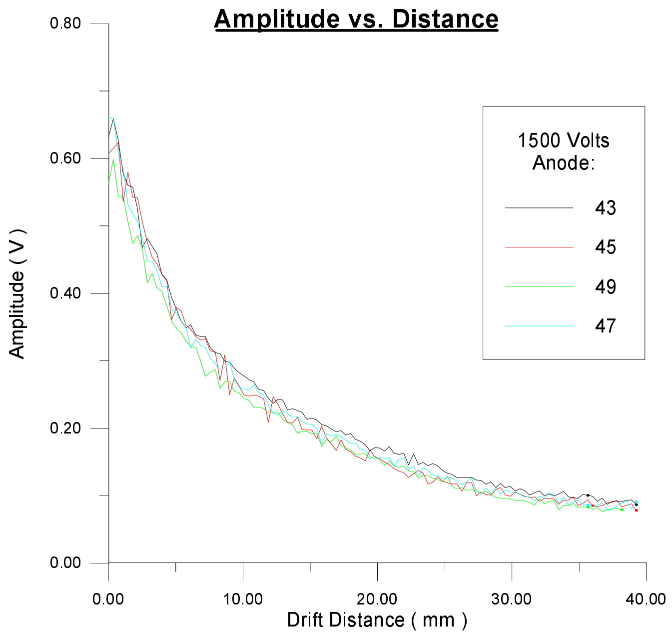

Figure 8: Measured pulse amplitude from the centered anode as a function of drift distance.

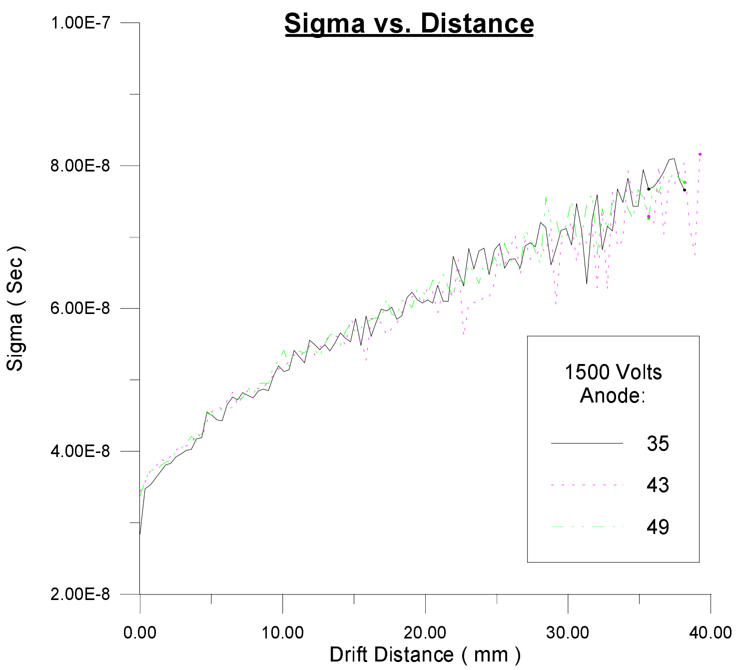

Figure 9: Measured signal width (σ) from the centered anode as a function of drift distance.

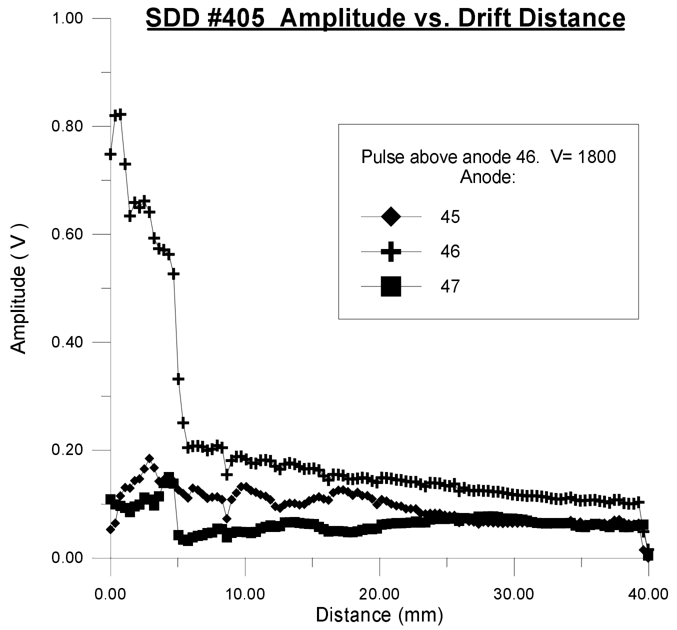

Figure 10: Signal amplitude as a function of drift distance for detector #405. Note the sharp drop in signal amplitude a drift distance of about 6mm.

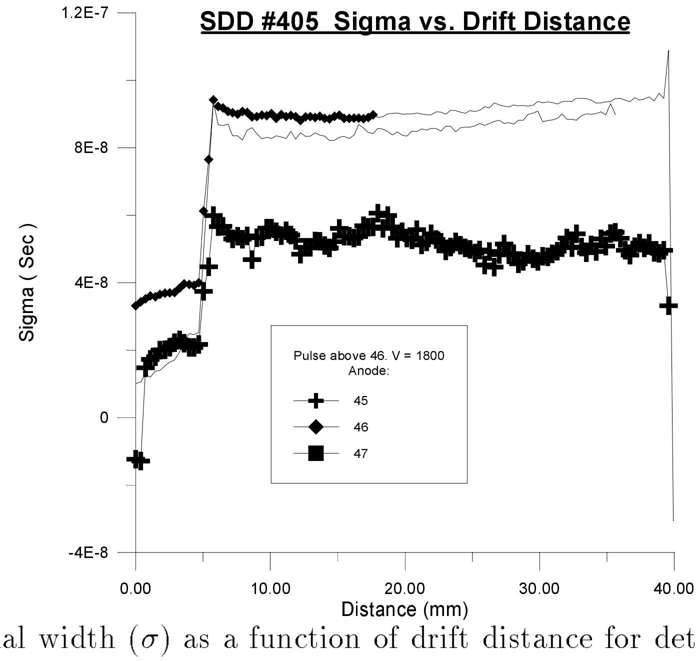

Figure 11: Signal width (σ) as a function of drift distance for detector #405. Note the abrupt rise in signal width a drift distance of about 6mm.

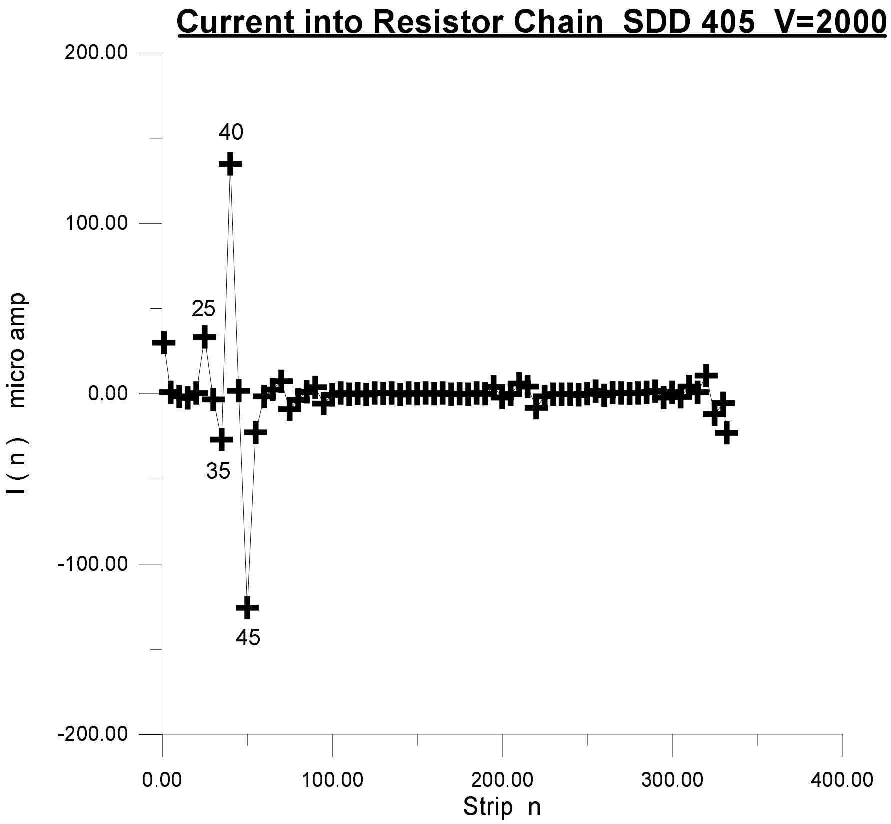

Figure 12: Current being supplied from the external resistor chain to detector #405 as a function of distance along the detector. The region of large current shown corresponds to the abrupt changes shown in previous figures.

results are shown in figures 13, 14, and 15. The change in the drift time follows that of the temperature. When the measured time of drift and temperature are plotted against one another (fig. 14) their correlation is even more obvious. We expect $v_{drift} \propto T^{-\alpha}$ [2] where α equals 2.4 and indeed the data in fig. 14 (and in other such data sets) reflects an α of nearly this value. The fact that we do not get exactly the expected value of 2.4 for α is at present more a reflection of thermal lag between where we measure the temperature and the temperature of the silicon itself than anything else. The scatter of the data around a straight line fit to the points in fig. 14 is shown in fig. 15. The precision of this detector is very good ($\approx 25\mu m$) but it is obvious that such precision can only be obtained if the temperature of the device is well controlled or monitored.

The effect of the lateral spread of the charge cloud is shown in figure 16. Shown is the response of the detector at a given anode as a function of the displacement of the laser spot laterally from the center of that anode. Assuming a Gaussian shaped distribution of charge in the drift and anode directions, the charge recorded should be represented by

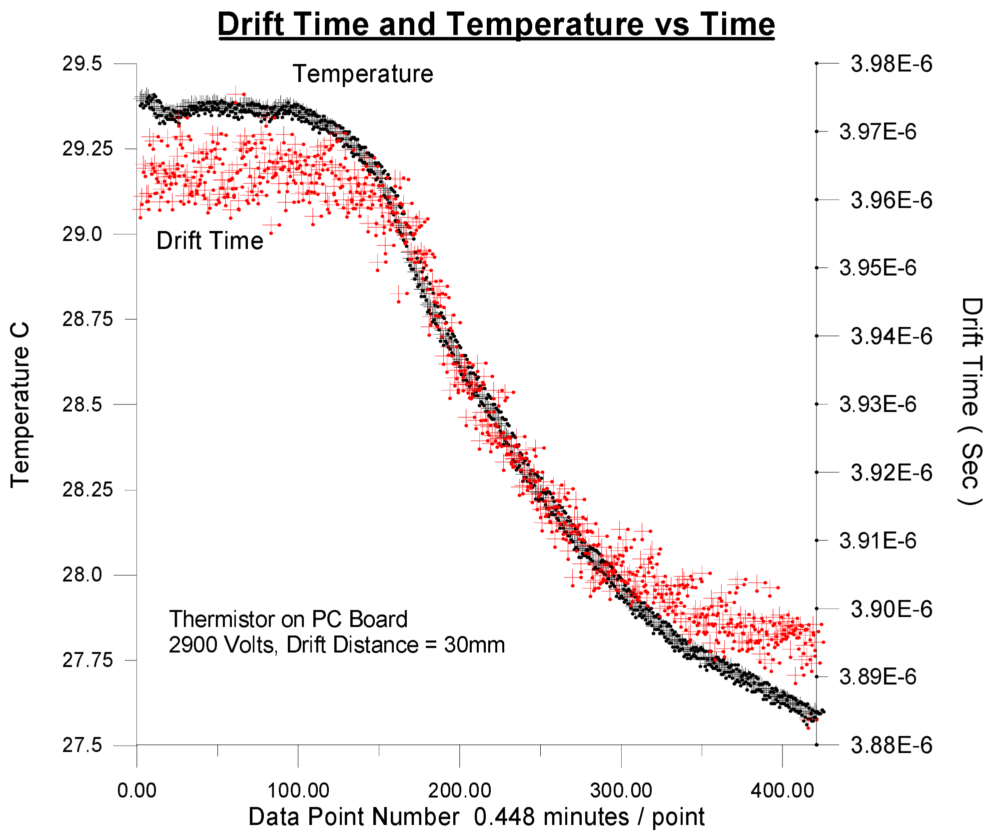

Figure 13: Variation of drift time and detector temperature over the course of several consecutive measurements. Note the correlation of drift time and temperature.

the following integral

$$Q_n(y_0, t) = \int_{-\Delta/2}^{+\Delta/2} \frac{Q_0}{\sigma_y\sqrt{2\pi}} e^{(y-y_0)^2/2\sigma_y^2}\, dy \ .$$

Where,

$$\sigma_y^2 = \sigma_{0y}^2 + 2D_y t$$

and $\Delta = 250\mu m$.

The different curves are from different initial drift distances and show a lateral width that grows as a function of drift distance.

The widths of this data as derived using the above expressions can be used to infer the diffusion constant of the electron drift cloud. Similarly in the drift direction, the sigma (fig. 9) from the fits to the pulse shape can also be used to infer the diffusion constant. The present results [3] give a diffusion constants of 4.2–4.7μm^2/ns in the lateral direction

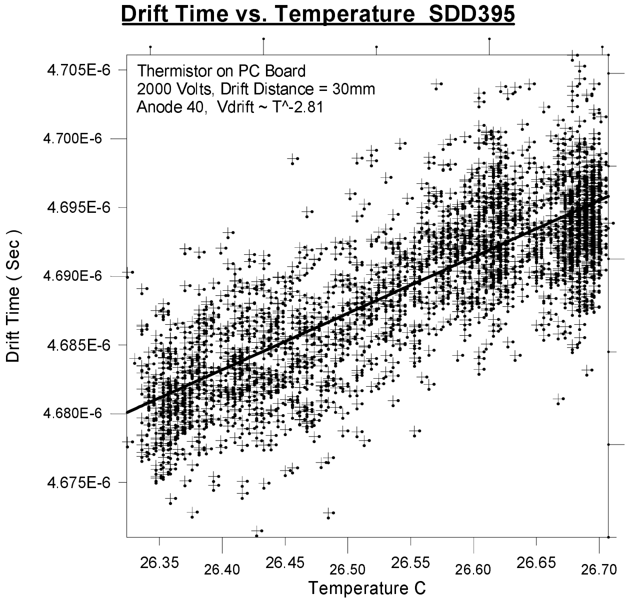

Figure 14: The correlation between drift time and temperature. The slope seen here is near the expected value. The difference may just reflect thermal lag between the detector itself and the thermistor.

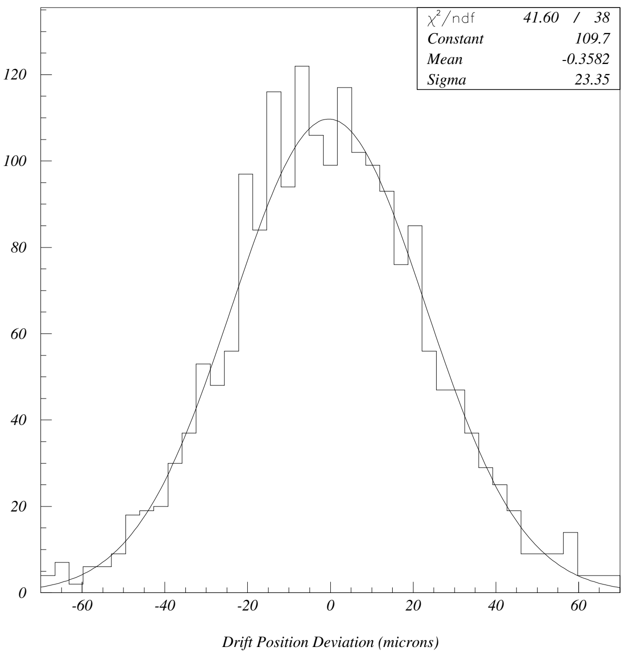

Figure 15: Scatter in the measured drift time after correction for temperature effects.

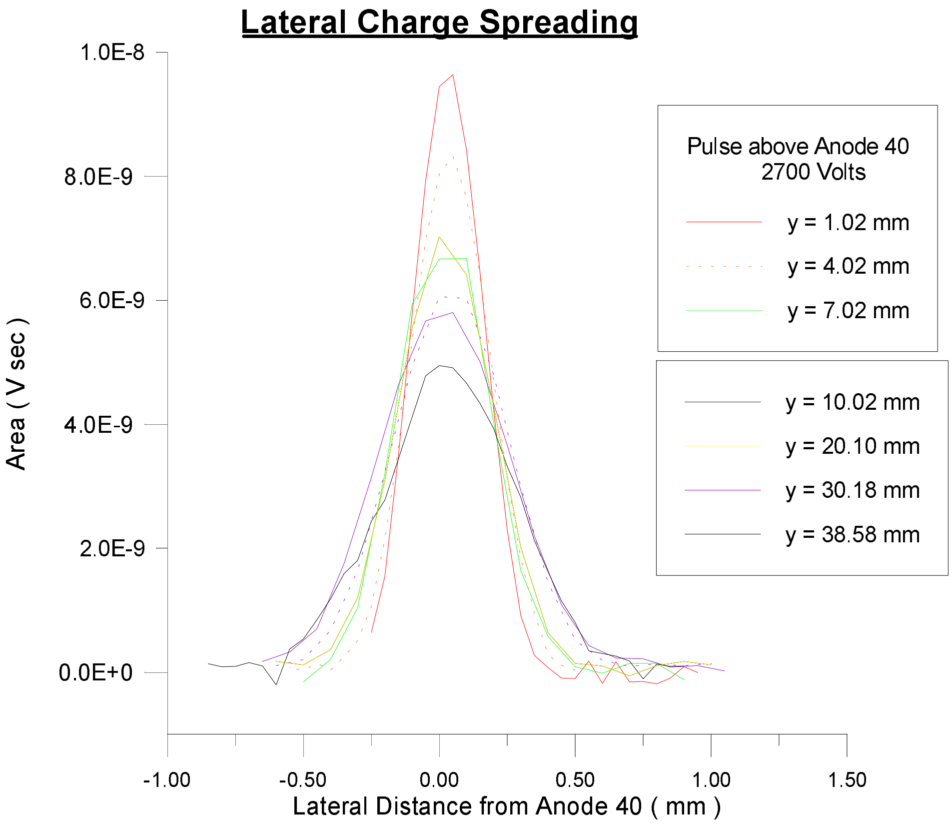

Figure 16: Charge collected in a single pad as a function of displacement of the injected charge from the center of that pad. The curves are for various distances of drift and evidence the lateral spreading of the charge cloud.

(larger than the expected 3.5μm^2/ns [2]) and $\approx$7.5μm^2/ns in the drift direction (about twice as large as expected). However, we note that for small drift distances the lateral width of the signal is not well fit by the above equation for a σ which contains only diffusion and no Coulomb term.

V. Rykov [3] has shown that for a "pancake"-like axially symmetric charge cloud, the evolution of the cloud width with time can be approximated by the following equation (neglecting the effect of image charges);

$$\frac{d\sigma^2(t)}{dt} = 2D + \frac{Q_0 \mu K}{\sigma(t)},$$

where Q_0 is the total charge in the electron cloud, μ is the electron mobility, and K is a coefficient depending on the cloud shape but independent of the width of the cloud for the case of a "steady" expansion where the electron density scales simply with time. However, fits to the data were not significantly improved by using near or asymptotic solutions to the above equation.

These problems may in part be understood by considering the effects shown in figure 18 (discussed later in the text). At each of the time dislocations shown in that figure, there is also a corresponding "jump" in the time width of the signal just as in the case of detector #405 (fig. 4) but much smaller in magnitude. Such "jumps", especially those close to the anode, could adversely affect the fits described above. Also one must bear in mind that in the drift direction it is the time width of the signal that is measured; while the width in length (μm) is inferred by assuming that the drift velocity is constant over the whole drift distance. In a drift field having a velocity of drift that is position dependent, the physical separation along the drift direction of any two drifting points is no longer a constant of their motion while their time-of-arrival difference at any location is.

In the case of a drift velocity that varies with position and under the assumption of piece wise linearity, one might make the approximation;

$$\frac{d\sigma_t^2}{dt} = \frac{2D}{{v_d}^2}$$

giving;

$$\sigma_t = \int_0^t \frac{2D}{v_d^2} dt = \int_0^x \frac{2D}{v_d^3} dx$$

where D is the diffusion constant, t the time of drift, and x the distance of drift. Here we assume that v_d never goes to zero. We effectively have a diffusion constant in *time* that is position dependent.

Such effects do not significantly change the drift time measurements but do seriously affect interpretation of the width measurements as there is no longer a simple linear relationship between drift time and the square of the drift width. We continue to try to better understand this part of our data and to obtain better and more consistent data.

The precision of the detector in the lateral direction (perpendicular to the drift direction) was also measured with a series of single shot measurements in a manner similar to that described above for the drift direction. The results are shown in figure 17 for a drift length of 20mm at an applied bias of 1500V. Assuming,

$$Q_n(y) = Q_0 e^{-y^2/2\sigma^2}$$

where y is the lateral displacement of the charge cloud from the center of anode n, then the charge in three anodes, Q_1, Q_2, and Q_3 can be used to infer the center and width (σ) of the charge cloud.

$$\sigma = \Delta \ln(\frac{Q_2^2}{Q_1 Q_2})^{-1/2}$$

$$y = \frac{\sigma^2}{2\Delta} \ln(\frac{Q_3}{Q_1})$$

Again Δ is the anode spacing of $250\mu m$. The measured lateral resolution is extremely good ($\sigma = 6\mu m$ here) but has yet to be measured at other distances and lateral displacements. The LBL group has obtained similar results at a closer distance.

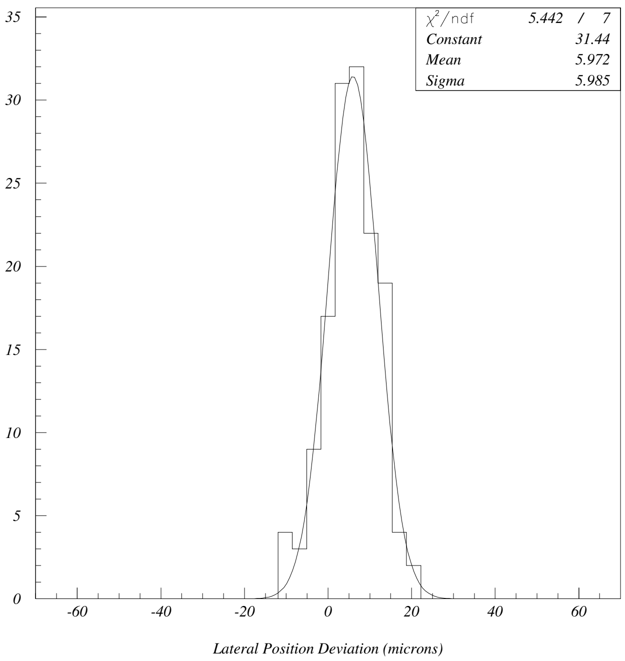

Figure 17: Scatter in the measured lateral position.

Differential Nonlinearity

The differential nonlinearity of the drift time vs distance curves for detector #395 is shown in figure 18.

A close examination of the drift time curves of detector #395 (fig. 3B) shows small deviations (jumps in time) from linearity. This is emphasized in figure 18 where the deviations of the drift time from a linear fit to the data are shown. These 'jumps' occur at exactly the same positions along the detector independent of whether the external voltage divider is used or not (compare figure 2B with figure 18); indicating that the problem is internal to the detector and not external to it. These small deviations are similar in form (but not magnitude) to the large deviation seen in detector #405 (fig. 4) At each of the large time jumps a corresponding jump can also be discerned in the measured widths of these signals, again similar to what is seen with detector #405. Also, the large 'jump' seen in detector #405 is at nearly the same distance as one of those shown in fig. 18. The cause of these nonlinearities is under investigation. We plan to do a detailed investigation of the bias of this detector searching for anomalies such as was seen for #405. Ultimately these deviations could be the limiting factor in the accuracy of position determination along the drift direction. The 'jumps' seen in figure 18 represent a much larger effect than the width shown in figure 15.

SCA – Digital Scope

To date, the results from tests at LBL using the switched capacitor array (SCA) and penetrating laser have been compatible with those from WSU except for the time resolution measurements. The signal widths in time (figures 9 and 15) measured at LBL

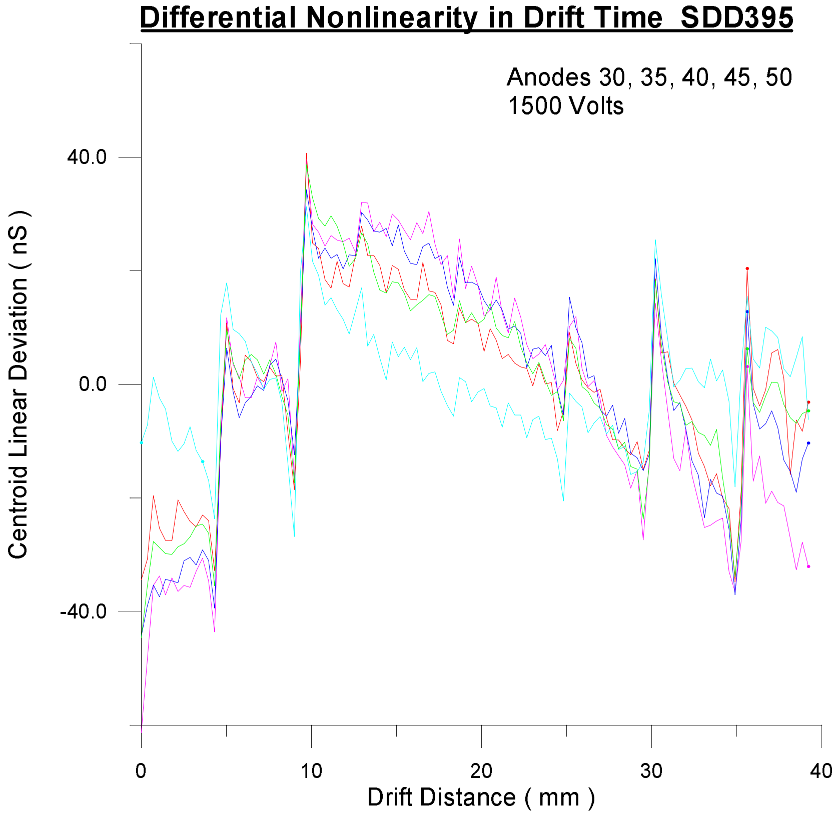

Figure 18: Measured differential nonlinearity of the drift time for detector #395.

are much larger than than those measured at WSU. The differences in these measurements are are believed to be caused by the loss of the precise start time of the laser pulse with respect to the clock of the SCA (modulo 25ns or perhaps 100ns). The digital scope with its finer time resolution does not have this problem. Because STAR will use an SCA read out with the same clock speed as that used at LBL (25ns) it is important to understand any differences that might occur. The problem of the precise start time (now precise event time) with respect to the SCA clock persists for STAR at RHIC and must be accounted for. A TDC referenced to the Beam–Beam counters and the SCA clock (or to Beam Crossing signal if the SCA clock is also referenced to it) would suffice to do the job but is necessary and must not be forgotten.

Summary

The present set of detectors have exhibited excellent precision in measurements at a fixed point both in the drift and pad directions. There is also evidence that charge recombination is negligible and can be ignored. The gross properties of these detectors are understandable and now our measurements are probing the detector on a finer scale.

In the near future we hope to have a complete set of parameters with which to characterize the response of these detectors. They will include among others the time evolution of the lateral and time widths, and the lateral precision measurements as a function of lateral offset and drift distance. We are also planing to do pulse pair resolution studies using two lasers pulsed at the same time. These are important to determine the effect of large particle densities on the detector performance. It is also very important that we examine in more detail the nonlinearities discussed above. This will involved a detailed mapping of the bias potential along the drift direction to measure any voltage irregularities that might exist. The results of these and other studies should prove valuable in designing the generations of detectors to come.

BNL is presently preparing to re-bond several SDDs allowing one half of the detector to be read out (90 anodes) at once. A VME based SCA read out system (LBL type) is assembled to for that purpose. Such a system will allow us to measure the large area characteristics of these detectors (are the present nonlinearities local or do they belong to a whole strip? what are the effects that occur near the guard areas?). It is also a step in the direction of becoming familiar with a large scale readout system for these detectors.

jrh

References

[1] E. Gatti and P. Rehak, Nucl. Instr. and Meth. 225 (1984) 608. and Nucl. Instr. and Meth. A235 (1985) 224.

[2] S.M. Sze, *Physics of Semiconductor Devices (2nd ed.)*, Wiley, New York, 1979

[3] V.L. Rykov et al., *SDD Signal Parameter Measurements*, Star Note #170 (1994).